

CMOS Readout Circuit with Wide Dynamic Range for an UV-NIR Silicon Sensor

Emmanuel Gómez-Ramírez, A. Díaz-Méndez,
Mariano Aceves Mijares, José Miguel Rocha Pérez,
and Jorge Miguel Pedraza Chávez

INAOE
Puebla, Mexico
e-mail: {emmanuelgomez, ajdiaz, maceves, jmr,
jpch}@inaoep.mx

Carlos Domínguez Horna, Ángel Merlos
IMB-CNM (CSIC)
Barcelona, Spain
e-mail: carlos.dominguez@imb-cnm.csic.es

Abstract— Currently, a CMOS imager capable of detecting from Ultraviolet-to-Near Infrared (UV to NIR) light is desirable. A new silicon sensor that detects from UV to NIR to be used for CMOS imaging was developed. However, the range of photo current generated by this sensor is wide. Then, there is a need to develop CMOS circuits with a wide dynamic range to be used with this sensor, or any other with wide output signal. This paper describes a CMOS readout circuit for applications in UV-NIR imaging with sensors that generate current in many orders of magnitude. The developed UV-NIR sensor is compatible with a CMOS technology. A new topology of a wide dynamic range readout circuit using a multimode sensing technique is proposed. Also, the design, computer simulation, and experimental corroboration are shown. It is demonstrated that automatic switching between different modes is achieved, and then a dynamic range up to 160 dB can be obtained.

Keywords-UV sensor; silicon sensor; smart-sensor; wide dynamic range; CMOS imagers; PWM sensors; continuously operating sensors; multimode sensing.

I. INTRODUCTION

Complementary Metal Oxide Semiconductor (CMOS) imagers capable of detecting from Ultraviolet-to-Near Infrared (UV to NIR) light is an area of research among the circuits and systems community. In our previous work [1], the design of an integrated circuit with a wide dynamic range was presented; this paper extends our results to show experimental feasibility.

Currently, CMOS technology allows the integration of complex electronic systems that include devices such as optical sensors. The integration of CMOS readout electronics and sensors allow the formation of CMOS imagers that offer several advantages compared to Charge-Coupled Device (CCD's) [2]. These include small power consumption, low voltage, low cost, etc., and have enabled the creation of imagers that represent single-chip solutions [2].

A CMOS imager capable of detecting radiation from UV to NIR is desirable for many applications in different areas, but these types of imagers have been difficult to implement due in part to the fact that silicon sensors have a reduced sensitivity in the UV light range when compared with the visible and NIR range.

To increase the response in the lower wavelength range it is necessary to use technologies that normally are not compatible with the CMOS technology, which generates difficulties for integration and extra cost.

A silicon detector sensible to UV light is reported in [3], which is compatible with CMOS technology [4]. This sensor increases the UV response, but it is necessary to have a readout system capable to respond in a wide range of currents, that is, the dynamic range has to be wide.

In order to have an integrated circuit that includes both the CMOS readout electronic functions and the mentioned sensor, two integrated circuits were designed. One of them has a CMOS 0.5 micrometer (μm) minimum feature with a new technique to improve the dynamic range and to face the problem of detecting currents from nanoamperes (nA) to microamperes (μA). The other one is done with 2.5 μm minimum feature CMOS technology. This technology is versatile enough to allow extra process steps to include the sensor fabrication.

Currently, both circuits are under fabrication. Moreover, it has been demonstrated that the sensor and the circuit can be built in the same process, 2.5 μm CMOS technology, with both conserving their characteristics [4]. On the other hand the design of the circuit with 0.5 μm technology was presented in [1].

In this paper, the design details and the experimental implementation of a CMOS pixel using the UV-NIR sensor and its acquisition circuitry with increased dynamic range to measure a wide range of currents are presented. The paper is divided into two sections; the first part corresponds to design details and the simulation of the integrated CMOS circuit with the 0.5 μm technology. The second part corresponds to the experimental section obtained using a discrete CMOS transistors implemented with Advanced Linear Devices (ALDs), which is a technique normally used to confirm the circuit design in a very economical way.

This paper is organized as follows: Section II presents the definition and basic assumptions of the multimode technique proposed and the design of the readout circuit. Sections III and IV present the results obtained in the simulation part and the experimental procedure of the proposed circuit, respectively. Section V summarizes the study.

II. PWM AND DIRECT MODE METHOD

In a CMOS imager, one of the most important figures of merit is the Dynamic Range (DR) [2] given by (1). The DR permits the differentiation between high and low excitation conditions in general, and, in the case of an image, between lightly and highly illuminated conditions.

It is clear that systems with higher DR would resolve extreme conditions without the loss of information.

$$DR = 20\log(V_{max}/V_{min}) \text{ [dB]}. \quad (1)$$

Many efforts have been made to obtain vision systems with wide DR. Different techniques to increase the DR have been reported; some of them are reviewed in [5-6] and are listed here: logarithmic method, clipping sensors, multimode sensors, frequency-based sensors, time-to-saturation sensors, multiple sampling methods, and multiple integration time methods.

As mentioned above, one technique to increase the DR is the multimode sensor. Multiple sensing techniques can be used in only one system to enhance the DR, by taking advantage of the best resolution of each one.

In this work, a multimode technique is used to increase the DR, with the combination of integration and direct mode detection methods.

In the first case (i.e., integration-based sensor or integration mode), photogenerated charges are integrated to produce a linear response. Using this method, current in the order of femtoamperes (fA) can be detected [7], corresponding to very small illumination intensities.

In the direct mode operated sensor technique, the current generated by a Photodiode (PD) is directly transferred to the measurement system. In this case, the current detected is in the order of nA to milliamperes (mA), corresponding to very high illumination intensities. Then, a combination of both readout techniques allows detecting the current of a PD from fA to mA.

A block diagram of the multimode technique used is shown in Fig. 1. As can be seen, the photocurrent from the sensor could be integrated in the upper branch (steps 1 to 3) or it could be amplified directly to the lower branch (steps 1 and 4).

In the integration mode, the photocurrent, I_{ph} , obtained in the step 1 (with the switch activated in the up position) is integrated and converted to a voltage ramp, step 2. In step 3, when the voltage ramp reaches the comparator reference voltage a shot pulse is obtained and this pulse controls the switch. In the direct mode, step 4, the I_{ph} is directly fed to an amplifier. Both readout signals are passed into a counter and an analog-to-digital converter respectively, and finally, in step 5, a Digital Word (DW) proportional to the incident light in the sensor is obtained.

Both techniques are explained with more details in next sections.

A. Pulse Width Modulation Mode Readout

When a sensor works in the integration mode, the parasitic capacitor of a PD is charged to a reference potential; when light shines on it, this potential decreases almost in a linear fashion, due to the photocurrent discharge of the capacitor.

By measuring the voltage drop, the amount of light received can be obtained, using (2), where I_{ph} is the photocurrent, T_{int} is the integration time, and C_{PD} is the parasitic capacitance of the PD.

$$\Delta V = I_{ph} * T_{int} / C_{PD}. \quad (2)$$

As it can be seen, ΔV is directly depend of T_{int} , so, it is necessary, a fine control over T_{int} to obtain an suitable output signal. To solve this, in Pulse Width Modulation (PWM) [8] mode, the current generated by each PD defines the integration time, T_{int} , so that very small are integrated until an adequate output is obtained.

In favor of greater clarity, in Fig. 1, integration mode is represented by steps 1 and 2, and PWM mode by steps 1 to 3. So, hereafter, the first part of the system (from steps 1 to 3) is referred as PWM mode and the second part (steps 1 and 4) as direct mode.

The circuit shown in Fig. 2 is an example of how to implement the PWM mode. The current is integrated and then compared with the reference voltage.

The P-type Metal Oxide Semiconductor (PMOS) transistor called Mrst in Fig. 2, works as a reset switch; in the ON state the PD voltage (V_{pd}) is near V_{dd} . If the switch is turned OFF, the incident light produces V_{pd} to decrease linearly.

When V_{pd} reaches the reference voltage, the comparator generates an output voltage pulse. Measuring the width of this pulse, the amount of light shining on the PD can be estimated.

The problem with this technique is that have limited DR. At higher levels of photocurrent, the integration time would be too short and in some cases imperceptible, restraining this method to low currents only. This technique works very well at small light power levels but fails to work adequately with high power levels, as shown in Fig. 3. In other words, a low illumination level produces a small photocurrent, as the light intensity is augmented the photocurrent increases reducing the integration time. If the light is intense, the integration time will be very difficult to measure.

To solve the high current problem bright light would be detected by direct mode technique.

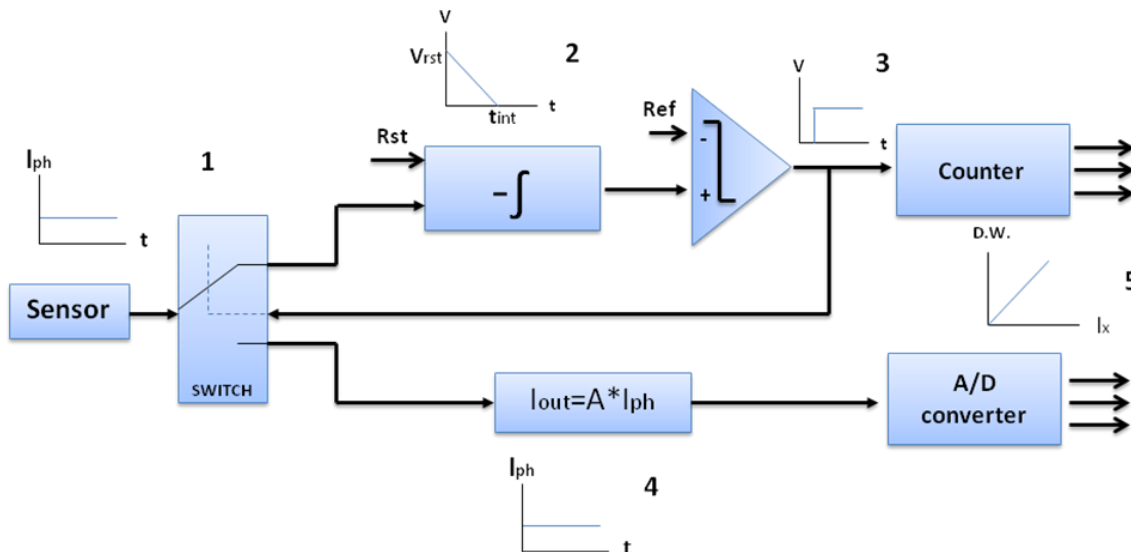


Figure 1. Multimode sensing block diagram.

B. Direct Mode Readout

In the direct output mode (or direct mode), the PD current is directly transferred to current mirrors with or without amplification. The disadvantage with this architecture is that suffers from low sensitivity at low levels of illumination; however, it works fine detecting high illumination levels.

Flipped-Voltage Follower (FVF) in current mode [9] is used to sense the PD current due to its very low input impedance and because it can drive large input current variations, as shown in Fig. 4. The FVF is shown in Fig. 4a; in this circuit, the input impedance Z_{in} is very low and given by

$$Z_{in} = 1/(g_{m1}g_{m2}r_{o1}). \tag{3}$$

where g_{m1} and g_{m2} are the transistor transconductances and r_{o1} is the transistor's output resistance in M1.

The input impedance is low due to the shunt feedback provided by M2. The output current is given by the expression $I_{out} = I_{ph} - I_{bias}$, where I_{bias} is the bias current provided by the current source in M1 and I_{ph} is the current from PD.

Normally, the current needs to be amplified so a current mirror is used and the gain is given by the ratio W/L of the transistors.

To make the mirrored current as accurate as possible it is necessary to use an operational amplifier, as shown in Fig. 4b, that keeps the bias voltage equal in the drains of M2 and M3.

Fig. 5 compares the fidelity of the current copy with and without the operational amplifier. As shown, the advantage of using the operational amplifier is clear.

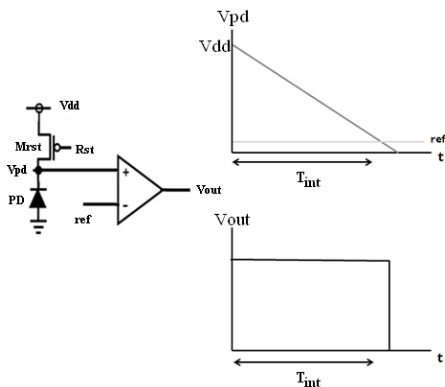


Figure 2. Circuit used to implement the PWM technique. The upper graph shows the V_{pd} voltage linear decay due to the incident light. The lower graph shows V_{out} as a function of time.

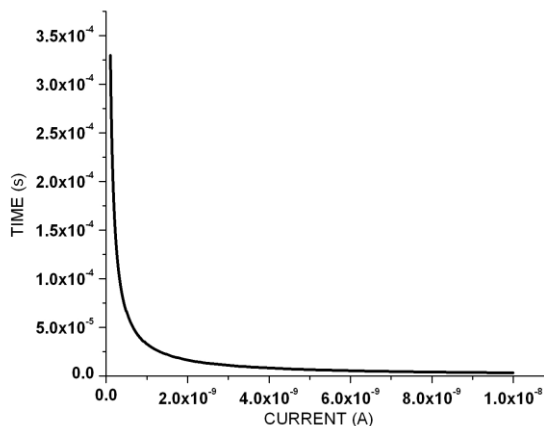


Figure 3. Photocurrent vs integration time; as the current increases the time tends toward zero.

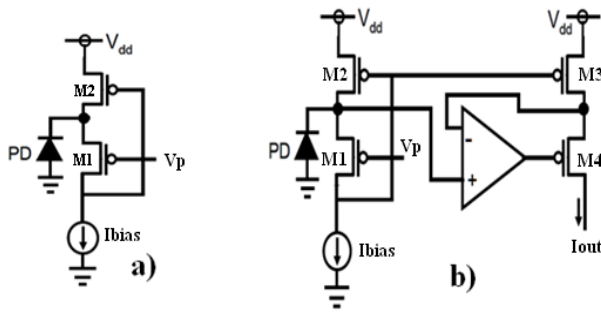


Figure 4. a) Flipped-Voltage Follower in current mode and b) with a current mirror.

C. PWM and Direct Mode Circuit Implementation

A schematic diagram of the proposed circuit is shown in Fig. 6, which combines both readout topologies: PWM and direct mode. When low illumination is shining on the PD, the PWM mode works, and when bright illumination is received, the direct mode topology comes into operation.

Internal switches that are controlled by the PWM output select one of the two topologies.

The PWM output voltage for a single sensor signal is shown in Fig. 7a; when the voltage ramp reaches the voltage reference a step is produced and the voltage gets a constant value. This voltage is then used to switch to the direct mode and the output current increases to a new value proportional to the current in the sensor, as shown in Fig. 7b.

As displayed in Figs. 2 and 6, an operational amplifier is needed in both topologies. So, sharing the operational amplifier in each pixel to run both techniques reduces the number of transistors and improves circuit performance.

III. CIRCUIT SIMULATION

Computer simulations of the circuit shown in Fig. 6 were performed, using HSPICE A-2008.03 [10]. The sensor was simulated using a simple photo-diode model, which consists of a voltage controlled current source in parallel with a capacitor and an exponential diode. The control voltage is proportional to the wavelength of the incident light in the sensor.

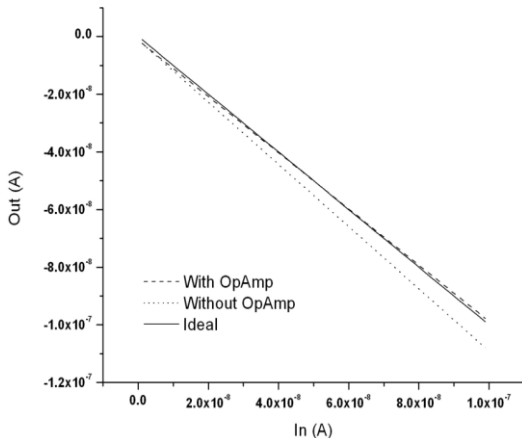


Figure 5. Input and output current comparison in the current mirror with and without the operational amplifier.

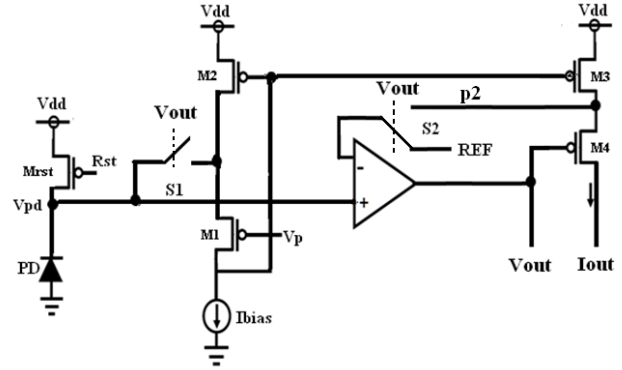


Figure 6. Dual mode circuit, when S1 and S2 are closed the direct mode is activated. When S1 is open and S2 is at the REF voltage, the PWM mode is activated.

Fig. 8 shows the results of simulations when dull incident light is cast on the sensor. As shown, the integration time starts when the reset command is triggered and V_{pd} is at V_{dd} (3.3V); then, different V_{pd} voltage ramps are produced by different light intensities. After some time, each ramp reaches the reference (in this case 1.5V). At that moment, the comparator output produces a voltage step.

This voltage step triggers the switches S1 and S2 to start the direct mode (switch S1 was off and S2 was in the REF position at the start), it is also used to bias the transistor, M4, allowing the I_{out} to increase to a value given by $(I_{ph}-I_{bias})$.

Fig. 8b shows the PWM output current; as can be seen, the current is zero until the voltage reference is reached then a high current is obtained. The elapsed period can be used to estimate the light intensity. In this case, the input current used was from 20 to 200 picoA (labels A and B correspond to the lower and the higher intensities, respectively).

Conversely, in Fig. 9, simulation results of the high current regime are shown.

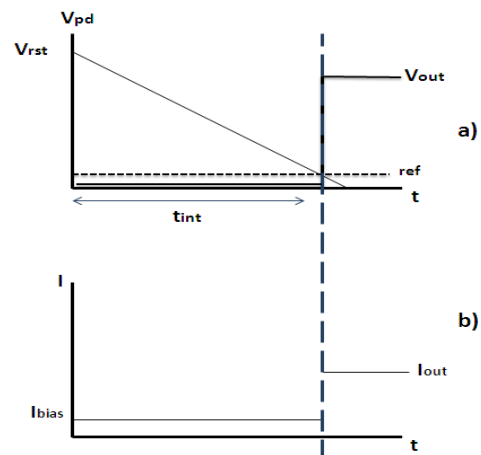


Figure 7. Output voltage and current of the PWM and direct mode sections. In a) the ramp of voltage is shown and after it reaches the reference a constant voltage step is produced. In b) as the PWM mode is active the I_{out} is low and when the direct mode is activated the I_{out} increases proportionally to the sensor's current.

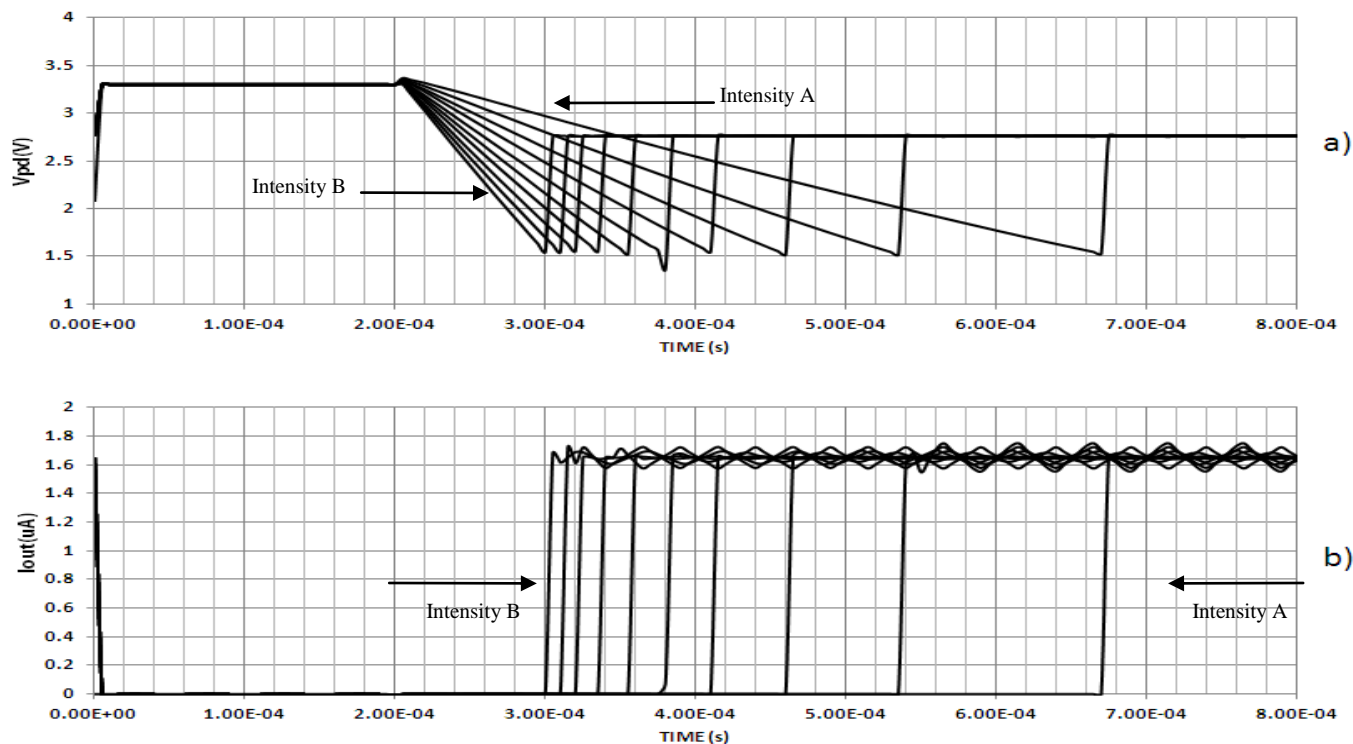


Figure 8. Simulation results of a low intensity light regimen, a) after 200us the V_{pd} linear decay starts and after reaching the reference a constant voltage is obtained; b) low intensities light sweep presents different integration time proportional to the light intensity.

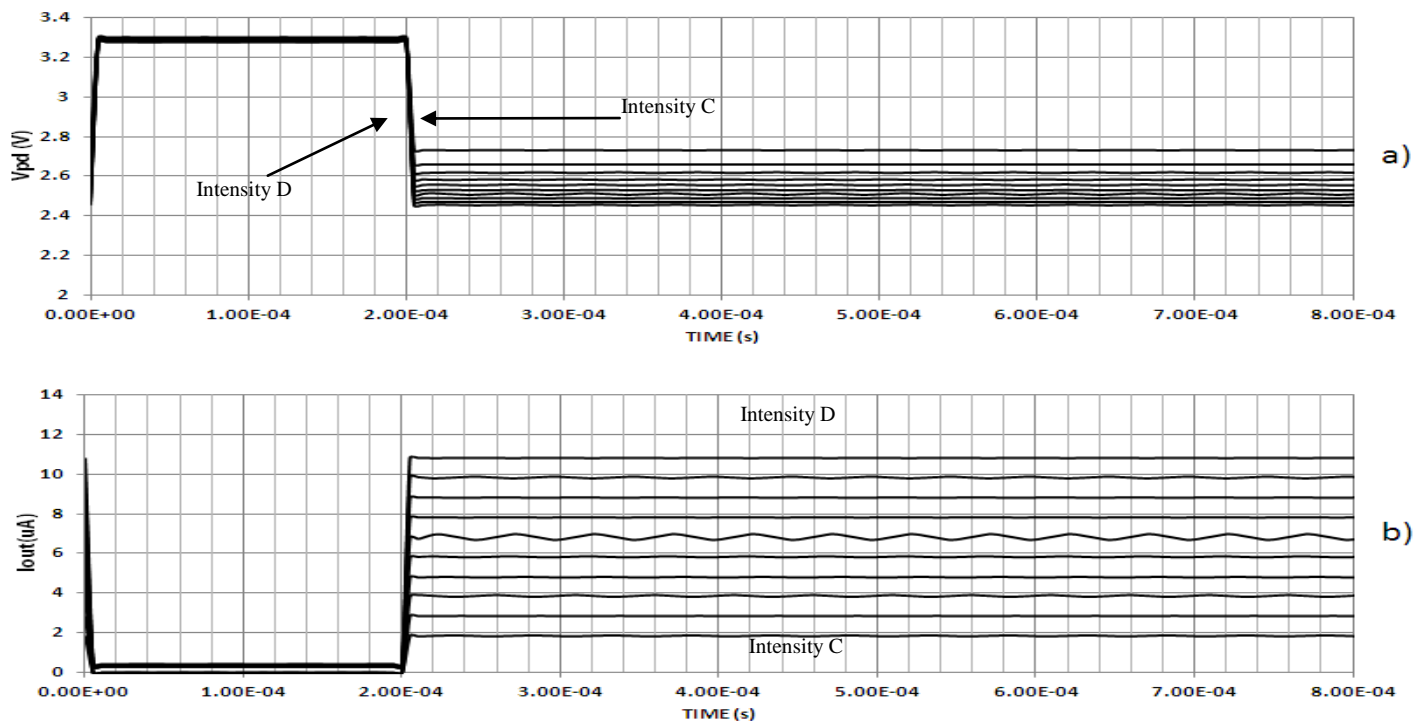


Figure 9. Simulation results of a high intensity light regimen, a) the V_{pd} linear decay is too fast and it is not differentiable due to the high current; then b) the current is measured in a straight forward manner.

In Fig. 9a, the PWM V_{out} is presented when the input currents varied from 50 to 500 nA. Labels C and D correspond to the lower and the higher intensities respectively. Comparatively in the results of Fig. 8a, after certain light intensity it is not possible to discriminate between the V_{out} ramps; intensities C and D cannot be differentiated. In this case, the output current is directly proportional to the current sensor and it is processed by the direct mode circuit. In Fig. 8b, the step of current is constant at a low value, approximately 1.6 μ A, and starts at different times; on the other hand, in Fig. 9a, the current steps are variable in amplitude and practically start at the same time. In this way, switches S1 and S2 are activated to select PWM or the direct mode.

The output current, I_{out} , is the difference of $I_{ph} - I_{bias}$, when the output voltage switches to the direct mode and when I_{ph} is higher than I_{bias} , a detectable I_{out} current is obtained. Therefore, the output current is used to estimate the light intensity.

Both topologies work for different illumination intensities; this allows increasing the DR. PWM topology working at tenuous light and direct current mode topology working at brighter illumination.

To measure the robustness of the design against process variations, 4-corners simulation is used submitting the circuit to extreme conditions.

Two examples of 4-corners simulation with 100 and 600 pA input current (labeled Typ1 and Typ2, respectively) using PWM mode readout are shown in Fig. 10; as can be seen in the first case (Typ1), the difference between the 4 simulations could be depreciate.

In the second case (Typ2), the maximum error was less than 5%, however, the variation in the voltage step is approximately 10%, due to the finite resistance of the switches. To solve this, an exhaustive study will be done to reduce the error using other topologies for the switches.

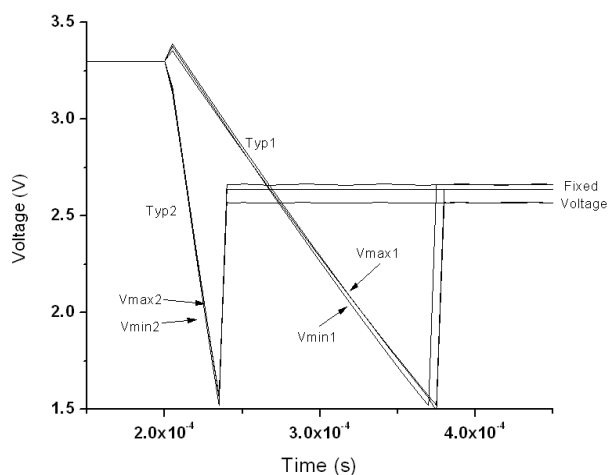


Figure 10. 4-corners simulation for PWM circuit with 100 and 600 pA input currents, for the low current regimen no difference is observed. The high regime current shows variations of 5% in the ramp voltage and 10% in the voltage step.

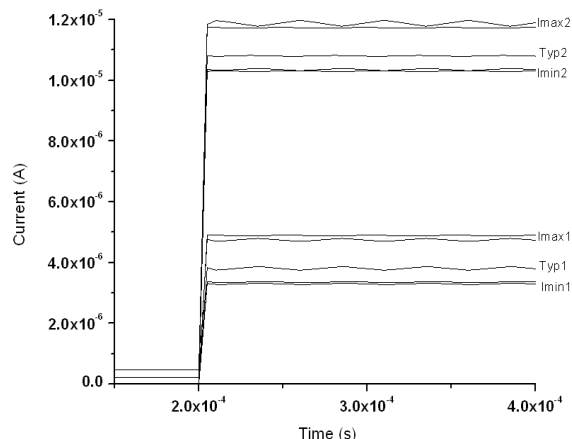


Figure 11. 4-corner simulation for direct mode circuit with 4 and 10 microA input currents; variations up to 10% are obtained.

Fig. 11 presents two examples of 4-corners simulation with 4 and 10 μ A input currents (labeled Typ1 and Typ2, respectively); in this case, direct mode readout is used. In both cases, the worst case variation was 10% reflecting the 10% variations of the V_{out} .

Fig. 12 presents V_{out} for the PWM circuit and I_{out} for the direct mode circuit. As can be seen in the low current regimen, the PWM works well up to 1×10^{-8} A; after this value, the output current starts to be measured directly. Consequently, the DR obtained in simulations is 160 dB, taking into account that the lower limit used to calculate it was the dark current of the photodiode.

The circuit was simulated using HSPICE, for a CMOS technology of 0.5 μ m from MOSIS; all the simulations presented here were post-layout simulations. Fig. 13 shows the layout of one pixel.

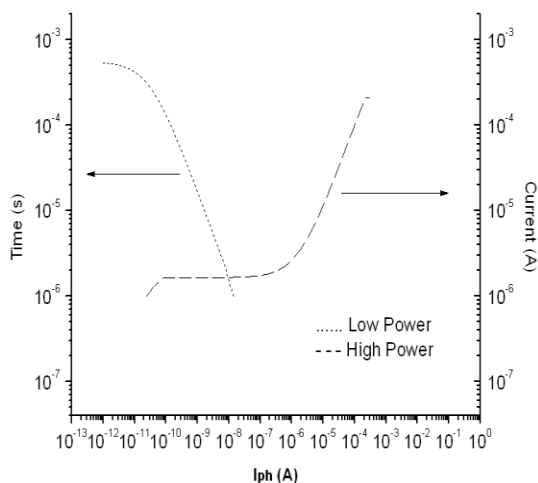


Figure 12. PWM and direct mode work ranges as function of photocurrent.

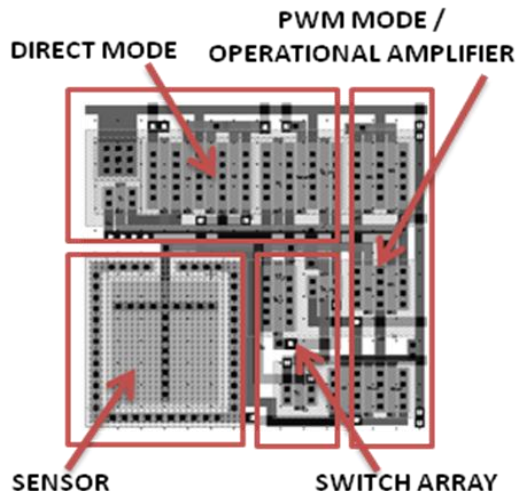


Figure 13. Layout of the PWM and direct mode circuit, using the 0.5 microns technology. The sensor area is 13x13 square microns and the total area is 50x50 square microns.

IV. EXPERIMENTAL CIRCUIT

In this section, experimental results are presented. First, the experimental procedure is explained. Second, results from characterization of UV sensor are presented. And finally, results from UV-ALD circuit with a variable source of light are presented.

A. Experimental Procedure

Currently, two integrated circuits are under fabrication: one is in a 2.5 microns technology and the other one is in 0.5 microns. The 2.5 microns technology is from CNM of Barcelona, Spain, and it allows modifying the process steps in order to integrate the sensor with the readout circuit. The compatibility of the sensor fabrication with a CMOS technology has been corroborated [4]. The 0.5 microns technology is from MOSIS. It is a standard technology and the same used in the simulation part. The MOS transistors used in the ALD arrays have characteristics similar to that of the MOSIS technology.

Experimentally, the circuit implementation was done using the quad N-channel matched pair MOSFET array ALD1106 [11] and the quad P-channel matched pair MOSFET array ALD1117 [12] with a discrete UV sensor.

The circuit in Fig. 6 was implemented with ALDs. The operational amplifier was accomplished using a Miller's model amplifier. Instead of PMOS transistor M_{rst} , an external master reset was used. The dimensions of the ALDs transistors are fixed, so, it was necessary to use ten transistors in parallel to implement the FVF with a gain of ten. Transistors like transmission gates were used to implement the switches that allow the change between PWM to direct mode. The circuit was biased with a voltage of 5V and a current of 2.5 μ A.

This discrete UV sensor was fabricated using a 2.5 microns technology. The sensor was not a standard Si PN junction; rather it incorporated special process steps during

its fabrication [13]. Four sensors of area 0.0015 cm² were built in the same chip and were packaged in a TO5. In this experiment, the four sensors were used simultaneously in parallel. Hereafter this arrangement is referred as "the sensor."

In order to characterize the sensor and the circuit from the 200 to 1000 nm wavelength range, the excitation light of a spectrofluorometer Horiba Jobin Yvon model FluorMax3 was used. The sensor was placed in a window normal to the light beam running from UV to NIR. To control the power intensity two configurations were used and referred to as: 5 slit and 15 slit. In order to do so the slit in the spectrofluorometer was in position 5 and 15.

Two measurements were done. First, the sensor current under different wavelengths was characterized. The spectrofluorometer was programmed to maintain each wavelength during 10 seconds and the current under each wavelength light was manually recorded using an electrometer Keithley model 6517A.

Next, the sensor was connected to the ALD circuit. The time and the current were measured from the outputs of the circuit. The output time was measured using an oscilloscope Agilent model 54622A and the current with the electrometer previously mentioned.

With this experimental setting the circuit implementation is expected to work as follows: when the master reset is turned on, the parasitic capacitor from the sensor is charged to V_{dd} , in this case 5V; when the excitation light from the spectrofluorometer illuminates the sensor and the master reset is turned off, a photocurrent from the sensor is generated. It is directly injected into the input of the FVF circuit implemented with ALD transistors, with the PWM topology enabled (S1 is turned off and S2 is in the REF position); this starts the discharge of the capacitor. When the voltage of the sensor reaches the reference voltage (2.5V) a step is generated in the output of the operational amplifier working as a comparator, V_{out} . The elapsed time (or output time), since the reset is turned off until the voltage step is generated, is recorded using the oscilloscope and this time is proportional to the current.

The step in V_{out} is used to switch from PWM to direct mode topology automatically (S1 is turned on and S2 change to position p2), this is when the direct mode is activated. So, the photocurrent is directly injected to the FVF and is amplified by the current mirror. After, the photocurrent is measured directly by the electrometer.

When the power intensity used is low, 5 slit, a fine work for the PWM topology is expected. On the other hand, when the lamp has 15 slit the direct mode topology will have a better performance.

Both topologies work at separate times. The PWM topology works first and when the step in V_{out} appears, the PWM topology is automatically disabled and the direct mode topology starts to work.

B. Experimental Results and Discussion

1) UV-NIR Silicon Sensor

As mentioned above, a sensor capable of detecting from UV-NIR light is presented in [3]. This sensor was characterized under different types of illumination. Basic characteristics of the sensor were measured under these illuminations, and are showed in next figures: Fig. 14 shows the dark current, which is approximately 2pA; the current from the sensor with two power excitations is shown in Fig. 15; the typical responsivity is shown in Fig. 16; and the capacitance versus reverse bias voltage is presented in Fig. 17.

As seen in Figs. 14 and 15, depending on the power of the optical input the circuit has to be able to discriminate currents in the range of pA to μ A.

2) Circuit

As is mentioned above, the UV-NIR sensor was connected to the arrangement and data obtained from the experiment are depicted in Table I, which shows: the current of the sensor (column “Current Sensor”); the output current of the current mirror (column “ $I_{out} - I_{bias}$ ”); and the output time, from reset off to the step in V_{out} (column “Time Tout”); for 5 and 15 slit.

As it can be seen, for 5 slit the output time is clearly and easily discernible. However, for 15 slit, the current is higher and hence it is better to measure it directly.

For example, analyzing the case when the wavelength is 400nm, with 5 slit, the current from the sensor is $0.711 \mu A$ and the output current is $4 \times 10^{-5} \mu A$, hence there is no comparison between them. In this case, it is necessary to use the output time to have an adequate output, which is easily discernable (in this case 180 us). On the other hand, when the intensity increase to 15 slit, it is better to take the output current, since it is $4.10 \mu A$, which agrees with the current from the sensor that is $4.290 \mu A$ and the output time is too small.

The different wavelengths used, have different intensities corresponding to the Xe lamp spectrum [14], but it is clear, from Table I, which variable (current or time) is better to use depending on the power of each wavelength.

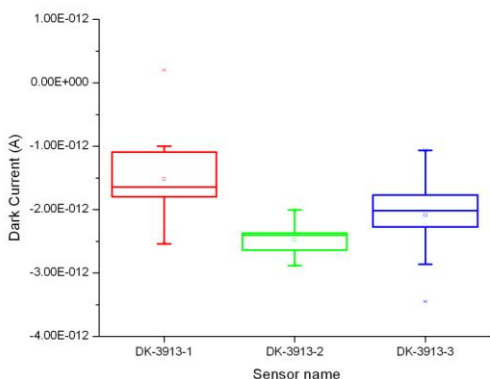


Figure 14. Dark current from different UV silicon photodiodes.

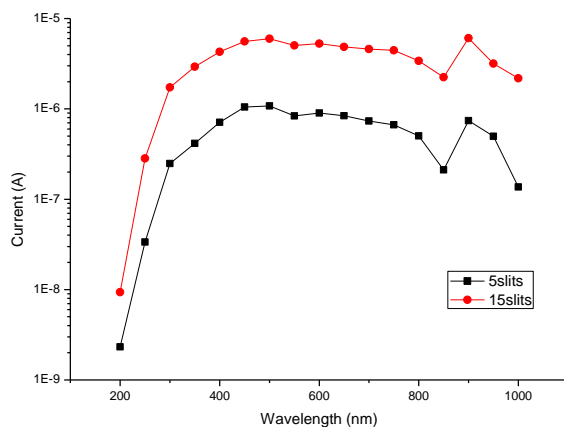


Figure 15. Typical UV sensor current as a function of wavelength for different optical power excitation.

TABLE I. DATA FROM SENSOR AND THE CIRCUIT IMPLEMENTATION FOR DIFFERENT LIGHT EXCITATIONS

Wavelength (nm)	5 slit			15 slit		
	Current Sensor (μA)	$I_{out} - I_{bias}$ (μA)	Time Tout (us)	Current Sensor (μA)	$I_{out} - I_{bias}$ (μA)	Time Tout (us)
200	0.002	0.000155	492	0.009	1.60	472
250	0.033	0.000155	416	0.283	1.20	288
300	0.248	0.000120	336	1.730	0.50	132
350	0.415	0.000085	228	2.930	2.40	68
400	0.711	0.000040	180	4.290	4.10	48
450	1.050	0.000010	152	5.590	5.70	36
500	1.080	0.000020	153	5.970	5.50	36
550	0.835	0.000040	156	5.040	4.80	36
600	0.900	0.000040	156	5.290	4.60	36
650	0.839	0.000030	156	4.860	4.80	36
700	0.735	0.000060	176	4.600	4.40	36
750	0.667	0.000070	192	4.450	3.60	44
800	0.503	0.000080	224	3.400	2.60	36
850	0.211	0.000120	316	2.240	1.20	92
900	0.740	0.000060	184	6.060	6.50	40
950	0.489	0.000090	232	3.170	2.20	72
1000	0.137	0.000095	368	2.180	0.80	104

To visualize better the different cases: when it is necessary the use one output (current) or the other one (time), figures 18-20 shows the discharge voltage of the capacitor and the output voltage for 5 and 15 slit, with different wavelengths.

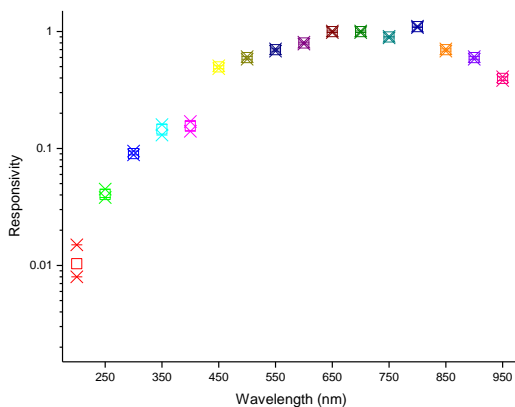


Figure 16. Typical responsivity of the sensor.

In Fig. 18, the fall off voltage of the parasitic capacitor of the UV sensor (when a beam of 200nm and 5 slit is applied) and the output signal from the comparator are shown.

In Figs. 19 and 20, the voltage in the PD and the output time are shown when the sensor is illuminated with different wavelengths but the same power intensity (5 slit). From this figure, it is clear that, for different light intensities, the current is different and that different time intervals are produced, which means the higher the current the shorter the output time.

The voltage in the PD and V_{out} as a function of time are shown in Figs. 21 and 22, respectively, but this time 15 slit was used. Comparing Figs. 19 and 20 with 21 and 22, it can be seen that the time out is shorter as the power is increased. This is a confirmation that as the power increases, the output time could be so short that it will be difficult to measure and differentiate a change in power or wavelength. In this case, for 15 slit it is hard to differentiate between 400, 600 and 800 nm, but for 5 slit it is difficult only to differentiate between 400 and 600 nm.

A comparison between the current from the sensor with the output of the circuit is shown. In Fig. 23, the comparison is for 5 slit, while in Fig. 24 it is for 15 slit, and it is confirmed that only for the high power case most of the points correspond.

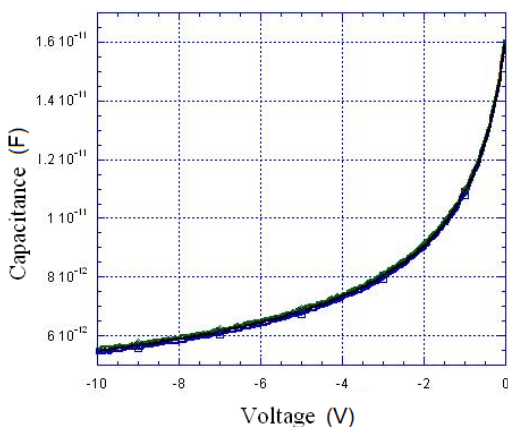


Figure 17. Typical capacitance VS reverse bias voltage.

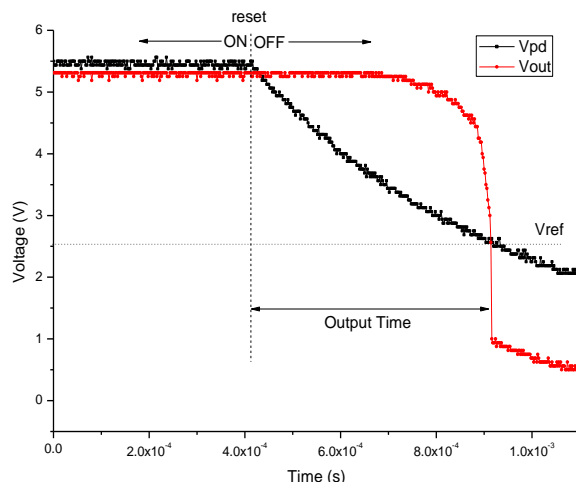


Figure 18. Output time and sensor decay voltage with a light excitation at the input of 200nm with 5slit

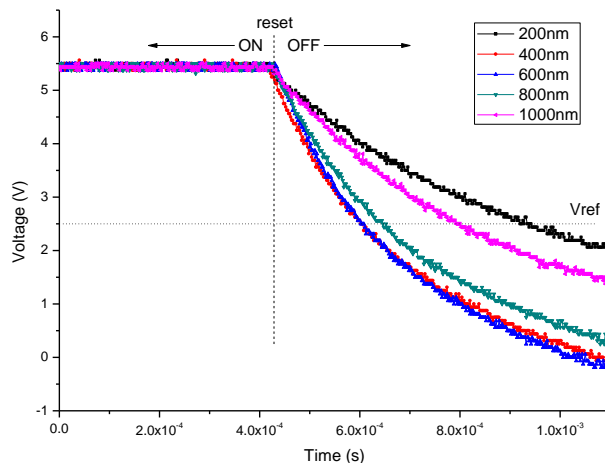


Figure 19. The discharge voltage of the capacitor as function of time is shown for different wavelengths. The input was illuminated with 5 slit.

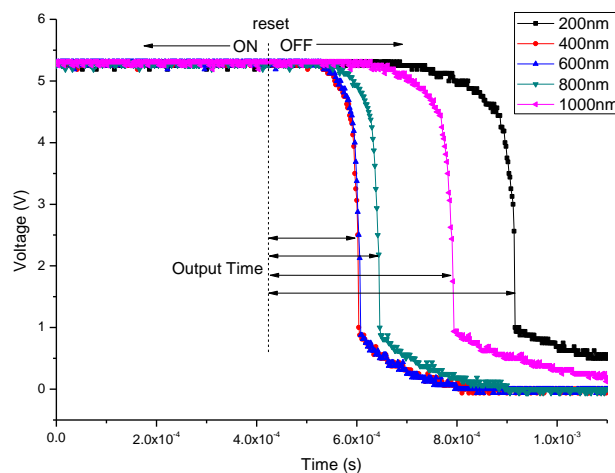


Figure 20. Output voltage for different wavelengths with 5 slit, the elapsed time for 200 nm is the largest time. The shortest elapsed time corresponds to the 400 nm wavelength, indicating that the blue color is the more intense in the Xenon lamp and produces the highest current in the sensor.

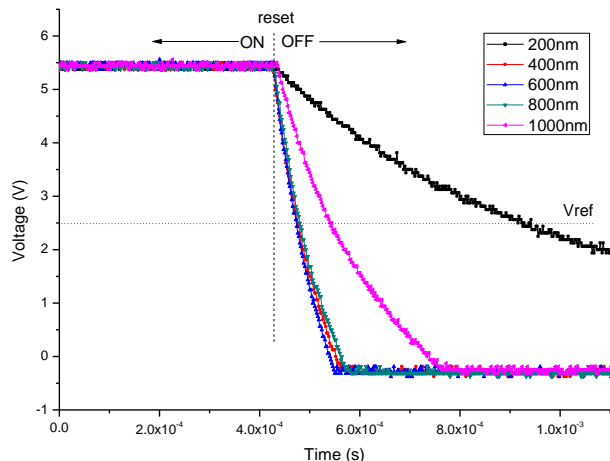


Figure 21. The discharge voltage of the capacitor as function of time is shown for different wavelengths. The input was illuminated with 15 slit.

It is clear that using the PWM and direct mode sequentially it is possible to sense low and high power signals. So, it has been proven experimentally that the circuit of Fig. 6 can be used to measure automatically very low and high currents with precision. The circuit has a total DR of 143 dB taking into account that the lower limit to calculate it was the intrinsic noise of the ALD circuits, and the upper limit was determined by the saturation current. Moreover, the DR can be incremented towards the upper limit, increasing the bias current, but this will cause an augment in the power consumption.

In Table II, a comparison between different topologies using the multimode techniques to increase DR is presented.

From this table it is inferred that only one, the Lineal-Logarithmic, reports a higher DR than the one presented here. However, the authors [17] used a smaller technology without reporting the power consumption.

Other articles present DR that exceeds the one reported here, but these works do not use the multimode technique nor the same technology [20]. Some reports do not mention the methods or techniques used to obtain a high DR [21].

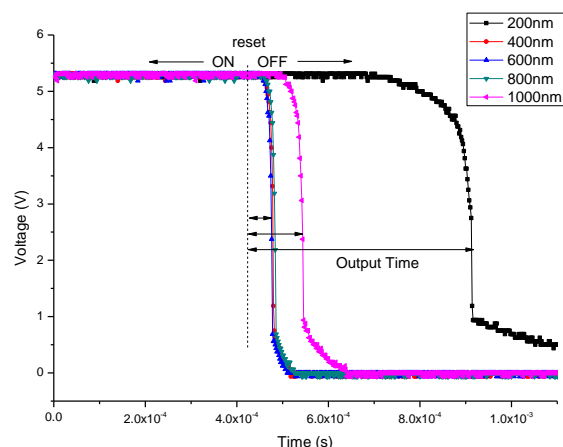


Figure 22. Output voltage for different wavelengths with 15 slit.

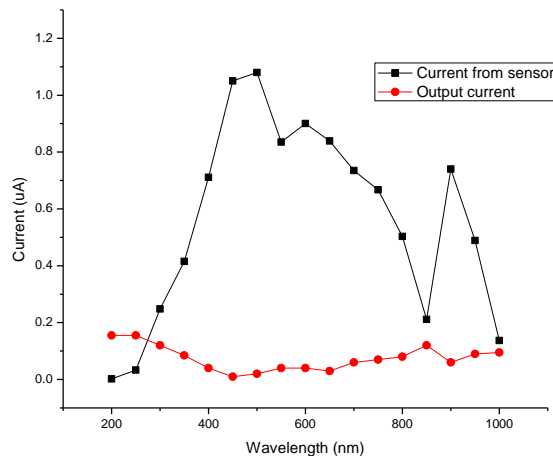


Figure 23. Comparison between the currents from the sensor and the circuit output currents with 5 slit.

TABLE II. MULTIMODE SENSING TECHNIQUES COMPARISON

	Specifications					
	Tech	DR	Area	Power Consumption	Year	Ref
Lineal – Logarithmic	0.35	124	7.5x7.5	---	2005	15
Lineal – Logarithmic	0.18	143	5.6x5.6	61mW y 84mW	2006	16
Lineal – Logarithmic	0.35	200	20x20	---	2006	17
Lineal – Logarithmic	0.35	112	9.4x9.4	---	2011	18
PWM – PFM	0.18	143	30x30	175mW	2011	19
PWM – Direct Mode	0.5	160	50x50	36 μW	---	This work
	ALDs	143	discrete	70 μW	---	

Another advantage to our approach is the improvement of the power consumption compared with those in Table II. This is because FVF working in current mode consumes negligible power.

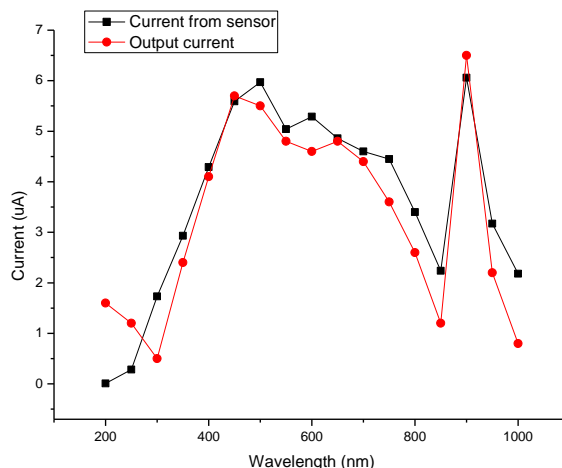


Figure 24. Comparison between the currents from the sensor and the circuit output currents with 15 slit.

V. CONCLUSIONS

A circuit that can be used in an integrated smart-pixel was designed, simulated and validated experimentally. It was corroborated that a wide dynamic range is achieved combining the pulse width modulation and direct current amplifications techniques in the same pixel; experimentally and by simulation, a DR of 143 dB and 160 dB were respectively obtained.

A reduced number of transistors were obtained sharing an operational amplifier by both techniques. The PWM and Direct mode are automatically selected depending on the range of current provided by the sensor. In the PWM mode the output time is used to estimate small photocurrents; in the direct mode high photocurrents are directly obtained. In comparison with similar circuits reported, the circuit proposed here improves the state of art.

In order to reduce area and power consumption, a single pixel circuit was designed using a 0.5 microns CMOS technology from MOSIS and occupying 50x50 square microns in total area.

The implementation with ALDs was tested in various wavelengths using a spectrofluorometer like the source of light.

Results show that the PWM topology works in cases when illumination is lower and the direct mode topology when is effective when it is higher.

Compared with other circuits reported in the literature, our approach has one of the highest DRs and smallest power consumptions, as demonstrated by the simulation.

ACKNOWLEDGMENT

The authors appreciate the English revision done by Rebekah Hosse Clark, also we appreciate the support of CONACyT.

REFERENCES

- [1] E. Gómez-Ramírez, A. Díaz-Méndez, M. Aceves-Mijares, J. M. Rocha-Pérez, J. M. Pedraza-Chávez, and C. Domínguez-Horna, "Wide dynamic range readout for cmos pixel using pwm and direct mode sensing techniques," in Proceedings of the Fourth International Conference on Sensor Device Technologies and Applications IARIA, Aug. 2013, pp 64-70, ISBN: 978-1-61208-297-4
- [2] J. Ohta, "Smart CMOS Image Sensors and Applications," CRC Press, 2008.
- [3] D. Berman-Mendoza, M. Aceves-Mijares, L. R. Berriel-Valdos, J. Pedraza, and A. Vera-Marquina "Fabrication, characterization, and optimization of an ultraviolet silicon sensor," Optical Engineering, vol. 47, no. 10, Oct. 2008, p. 104001, doi:10.1117/1.3000434
- [4] M. Aceves-Mijares, E. Gómez-Ramírez, A. Díaz-Méndez, J. M. Rocha-Pérez, J. M. Pedraza-Chávez, J. Alarcón-Salazar, S. Román-López, C. Domínguez-Horna, A. Merlos, X. Formatjé, and A. Morales-Sánchez "Conservation of the optical properties of sro after cmos IC processing," in press.
- [5] A. Spivak, A. Belenky, A. Fish, and O. Yadid-Pecht "Wide-dynamic-range cmos image sensors: comparative performance analysis," IEEE Transactions on Electron Devices, vol. 56, no. 11, Nov. 2009, pp. 2446-2461.
- [6] D. Park, J. Rhee, and Y. Joo "A wide dynamic-range cmos image sensor using self-reset technique," IEEE Electron Device Letters, vol. 28, no. 10, Oct. 2007, pp. 890-892.
- [7] B. Goldstein, D. Kim, A. Rottigni, J. Xu, T. K. Vanderlick, and E. Culurciello "Cmos low current measurement system for biomedical applications," IEEE International Symposium on Circuits and Systems (ISCAS), May 2011, pp. 1017-1020.
- [8] A. Zarándy, "Focal-Plane Sensor-Processor Chips," Springer, 2011.
- [9] R. González-Carvajal, J. Ramírez-Angulo, A. J. Lopez-Martin, A. Torralba, J.A. Gómez-Galan, A. Carlosena, and F. Muñoz-Chavero, "The flipped voltage follower: a useful cell for low voltage low power circuits design," IEEE Transactions On Circuits And Systems, vol. 52, no. 7, Jul. 2005, pp. 1276-1291.
- [10] Synopsys, "HSPICE", URL: <http://www.synopsys.com/>, 2013.
- [11] N-channel MOSFET, URL:<http://html.alldatasheet.net/html-pdf/55017/ALD/ALD1106/46/1/ALD1106.html>, 2014.
- [12] P-channel MOSFET, URL:<http://html.alldatasheet.es/html-pdf/55019/ALD/ALD1117/46/1/ALD1117.html>, 2014.
- [13] D. Berman-Mendoza, M. Aceves-Mijares, L. R. Berriel-Valdos, J. Carranza, J. Pedraza, C. Domínguez-Horna, and C. Falcony "Silicon-rich silicon oxide films boost UV sensitivity," Laser Focus World, vol. 41, no. 9, Sept. 2005, p.103.
- [14] Fluoro max-3 operation manual, URL:<http://www.jobinyvon.com>, 2013.
- [15] K. Hara, H. Kubo, M. Kimura, F. Murao, and S. Komori "A linear-logarithmic cmos sensor with offset calibration using an injected charge signal," IEEE International Solid-State Circuits Conference, vol. 1, Feb. 2005, pp. 354-603.
- [16] G. Storm, R. Henderson, J. E. D. Hurwitz, D. Renshaw, K. Findlater, and M. Purcell "Extended dynamic range from a combined linear-logarithmic cmos image sensor," IEEE Journal of Solid-State Circuits, vol. 41, no. 9, Sept. 2006, pp. 2095-2106.
- [17] N. Akahane, R. Ryuzaki, S. Adachi, K. Mizobuchi, and S. Sugawa "A 200dB dynamic range iris-less cmos image," IEEE International Solid-State Circuits Conference, Feb. 2006, pp. 1161-1170.
- [18] M. Vatteroni, P. Valdastrì, A. Sartori, A. Menciassi, and P. Dario "Linear-logarithmic cmos pixel with tunable dynamic range," IEEE Transactions On Electron Devices, vol. 58, no. 4, Apr. 2011, pp. 1108-1115.
- [19] C. Posch, D. Matolin, and R. Wohlgenannt "A qvga 143 dB dynamic range frame free pwm image sensor with lossless pixel," IEEE Journal Of Solid-State Circuits, vol. 46, no. 1, Jan. 2011, pp. 259-275.
- [20] N. Ide, W. Lee, N. Akahane, and S. Sugawa "A wide DR and linear response cmos image sensor with three photocurrent integrations in photodiodes, lateral overflow capacitors, and column capacitors," IEEE Journal Of Solid-State Circuits, vol. 43, no. 7, Jul. 2008, pp. 1577-1587.
- [21] Electronic Publication: Omron Corporation: "German venture company develops highly advanced wide dynamic range cmos image sensor," [Online]. URL: <http://industrial.omron.fr/fr/news/news/cmos-image-sensor>, 2003.